Modulational Instability of the Higher-Order Nonlinear Schrödinger Equation with Fourth-Order Dispersion and Quintic Nonlinear Terms

Woo-Pyo Hong

Department of Electronics Engineering, Catholic University of Daegu, Hayang, Gyongsan, Gyungbuk 712-702, South Korea

Reprint requests to Prof. W.-P. H.; E-mail: wphong@cu.ac.kr

The modulational instability of the higher-order nonlinear Schrödinger equation with fourth-order dispersion and quintic nonlinear terms, describing the propagation of extremely short pulses, is investigated. Several types of gains by modulational instability are shown to exist in both the anomalous and normal dispersion regimes depending on the sign and strength of the higher-order nonlinear terms. The evolution of the modulational instability in both the anomalous and normal dispersion regimes is numerically investigated and the effects of the higher-order dispersion and nonlinear terms on the formation and evolution of the solitons induced by modulational instability are studied. – PACS numbers: 42.65.Tg, 42.81Dp, 42.65Sf

1. Introduction

Modulational instability (MI), occuring as a result of an interplay between the nonlinearity and dispersion (or diffraction, in the spatial domain), is a fundamental and ubiquitous process that appears in most nonlinear wave systems in nature such as fluid dynamics [1, 2], nonlinear optics [3, 4], and plasma physics [5]. As a result, a continuous-wave (CW) or quasi-CW radiation propagating in a nonlinear dispersive medium may suffer the instability with respect to weak periodic modulations of the steady state and results in the breakup of CW into a train of ultrashort pulses [6]. In the context of fiber optics, the temporal MI has been experimentally verified for a single pump wave propagating in a standard non-birefringence fiber, which can be modeled by the nonlinear Schrödinger (NLS) equation, and it was found that the MI only occurs in the anomalous group-velocity dispersion (GVD) regime with a positive cubic nonlinear term [6, 7]. On the other hand, in the context of the vector NLS equations which can describe two or more optical fields copropagating inside the highly birefringence optical fibers, MI can also exist in the normal dispersion regime as the result of a novel phenomenon called the cross-phase modulation (XPM) [8]. The purpose of the present work is to show that MI can also occur in both anomalous and normal

dispersion regimes and to study the dynamics of the MI induced solitons in the context of an extended higher-order NLS equation.

As the extended higher-order NLS equation we consider the generalized NLS with a third- and fourth-order dispersion and cubic-quintic nonlinear terms, describing the propagation of intense femtosecond optical pulses in a medium which exhibits a parabolic nonlinearity law [6, 9 – 12], in the form of

$$
\frac{\partial A}{\partial z} + \frac{i}{2}\beta_2\frac{\partial^3 A}{\partial \tau^2} - \frac{1}{6}\beta_3\frac{\partial^3 A}{\partial \tau^3} - \frac{i}{24}\beta_4\frac{\partial^4 A}{\partial \tau^4} + \frac{\alpha}{2}A =
$$
$$
i\gamma_1|A|^2A + i\gamma_2|A|^4A - \frac{\gamma_1}{\omega_0}\frac{\partial(|A|^2A)}{\partial \tau} - i\gamma_1 T_R A\frac{\partial|A|^2}{\partial \tau}.
$$

(1)

Here $A(z,\tau)$ is the slowly varying envelope of the electromagnetic field, $\tau \equiv t - \beta_1 z$ is the retarded time, $\beta_j \equiv (\mathrm{d}^2 k_j/\mathrm{d}\omega^2)_{\omega=\omega_0}$ ($j=2,3,4$) are the GVD coefficients evaluated at the carrier frequency ω_0, the attenuation term corresponding to the fiber loss α, and γ_1 and γ_2 are the nonlinear coefficients. The term proportional to γ_1/ω_0 results from the intensity dependence of the group velocity and causes self-steepening and shock formation at the pulse edge. The last term represents the intrapulse Raman scattering, which causes a self-frequency shift, where T_R is related to the slope

of the Raman gain [6]. Some analytic bright solitary-wave solutions of (1) in the anomalous and normal dispersion regimes in the absence of the self-steepening and the Raman scattering terms were obtained under various constraints among the coefficients, and the effects of the third- and fourth-order dispersion terms on the dynamics of solitary-waves were numerically studied [9, 10].

Shagalov [13] has investigated the effects of the third- and fourth-order dispersion terms, in the absence of the quintic nonlinear term ($\gamma_2 = 0$) and the self-steepening and the Raman terms of (1), on the MI and showed that modulationally unstable waves evolve to soliton-type or turbulent states depending on the strength of the higher-order dispersion terms. Recently, the author [14] has obtained the exact analytic expression for the gain by the MI and numerically studied the dynamics of the solitons induced by the MI of (1) in the absence of the self-steepening and Raman terms. It was shown that solitons exist both for the anomalous and the normal dispersion regimes and in particular the role of the third-order dispersion term β_3 on the evolution of the MI was analyzed. More recently, in the context of (1) without the quintic nonlinear term, Demircan and Bandelow [12] have numerically verified the supercontinuum generation by the MI in the anomalous as well as in the normal dispersion region, which has been experimentally observed [15]. They showed that the MI dominates higher-order effects such as third- and fourth-order dispersion, self-steepening and stimulated Raman scattering. However, the self-consistent investigation on the MI of (1) and the dynamics of the solitons induced by the MI have not been performed, which will be pursued in the present work.

The paper is organized as follows. In Section 2, we obtain the analytic expressions for the gain by MI and show that the inclusion of the fourth-order dispersion and quintic nonlinear terms leads to a more complicated gain spectrum than those of [13, 14, 16, 17]. Subsequently, we show that the MI gain can also occur even in the normal dispersion regime, depending on the sign and strength of the higher-order dispersion and the nonlinear terms. In Section 3, we then numerically investigate the dynamics of the initial steady CW in the anomalous and normal dispersion regimes under a weak modulational field with a modulation frequency obtained from the MI gain spectra. In particular, the effect of the third-order dispersion and cubic-quintic nonlinear terms on the evolution of MI is studied. The conclusions follow in Section 4.

2. Gain by the Modulational Instability

In order to investigate how weak and time-dependent perturbations evolve along the propagation distance, we consider the following linear stability analysis. The steady-state solution of (1) is given by

$$\bar{A}(z,\tau) = \sqrt{P}\exp(i\phi_{\mathrm{NL}}), \qquad (2)$$

where the nonlinear phase shift ϕ_{NL} is related to the optical power P and the propagation distance z as $\phi_{\mathrm{NL}} = (i\alpha/2 - \gamma_1 P - \gamma_2 P^2)z$. The linear stability of the steady-state can be examined by introducing a perturbed field of the form

$$A(z,\tau) = [\sqrt{P}+\varepsilon(z,\tau)]\exp[-\frac{\alpha}{2}z-i(\gamma_1 P+\gamma_2 P^2)z], \quad (3)$$

where the complex field $|\varepsilon(z,\tau)| << \sqrt{P}$. Thus, if the perturbed field grows exponentially, the steady-state becomes unstable. By substituting (3) into (1) and collecting terms in ε, we obtain the linearized equation as

$$\begin{aligned}
&\varepsilon_z - (2\frac{\gamma_1 P}{\omega_0} + i\gamma_1 T_{\mathrm{R}}P)\varepsilon_t - (\frac{\gamma_1 P}{\omega_0} + i\gamma_1 T_{\mathrm{R}}P)\varepsilon_t^* \\
&\quad - \frac{1}{24}i\beta_4\varepsilon_{tttt} + \frac{1}{2}i\beta_2\varepsilon_{tt} - \frac{1}{6}\beta_3\varepsilon_{ttt} \\
&\quad + i(\gamma_1 P + 2\gamma_2 P^2)(\varepsilon + \varepsilon^*) = 0,
\end{aligned} \qquad (4)$$

where $*$ denotes complex conjugates. We assume a general solution of the form

$$\varepsilon(z,\tau) = U\exp[i(Kz-\Omega\tau)]+V\exp[-i(Kz-\Omega\tau)], \quad (5)$$

where K and Ω represent the wave number and the frequency of the modulation [6], respectively. Inserting (5) to (4), we obtain the dispersion relation

$$K^2 + C_k K + \Phi_8\Omega^8 + \Phi_6\Omega^6 + \Phi_4\Omega^4 + \Phi_2\Omega^2 = 0, \quad (6)$$

where

$$C_k \equiv C_{k,r} + iC_{k,i} = -\frac{1}{3}\beta_3\Omega^3 + 4\frac{\gamma_1 P\Omega}{\omega_0} + 2i\gamma_1 T_{\mathrm{R}}P\Omega,$$

$$\Phi_8 = -\frac{1}{576}\beta_4{}^2,$$

$$\Phi_6 = -\frac{1}{24}\beta_4\beta_2 + \frac{1}{36}\beta_3{}^2,$$

$$\Phi_4 \equiv \Phi_{4,r} + i\Phi_{4,i} = -\frac{1}{4}\beta_2{}^2 - \frac{2}{3}\frac{\beta_3\gamma_1 P}{\omega_0}$$

$$\quad + (\frac{1}{12}\gamma_1 P + \frac{1}{6}\gamma_2 P^2)\beta_4 - \frac{1}{3}i\beta_3\gamma_1 PT_{\mathrm{R}},$$

$$\Phi_2 \equiv \Phi_{2,r} + i\Phi_{2,i} = (2\gamma_2 P^2 + \gamma_1 P)\beta_2$$

$$+ 3\frac{\gamma_1^2 P^2}{\omega_0^2} + i\frac{2\gamma_1^2 P^2 T_R}{\omega_0}. \tag{7}$$

The dispersion relation has the solution

$$K = -\frac{1}{2}C_{k,r} - \frac{1}{2}iC_{k,i} \pm \frac{1}{2}\sqrt{\Xi + i\Delta},$$

$$\Xi = C_{k,r}^2 - C_{k,i}^2 - 4\Omega^2\Phi_{2,r} - 4\Omega^4\Phi_{4,r}$$

$$- 4\Phi_6\Omega^6 - 4\Phi_8\Omega^8, \tag{8}$$

$$\Delta = (2C_{k,r}C_{k,i} - 4\Omega^2\Phi_{2,i} - 4\Omega^4\Phi_{4,i})$$

or

$$K = -\frac{1}{2}C_{k,r} - \frac{1}{2}iC_{k,i} \pm \frac{1}{2}\left[(\Xi^2 + \Delta^2)^{1/4}\cos\left(\frac{\alpha}{2}\right)\right.$$

$$\left. + i(\Xi^2 + \Delta^2)^{1/4}\sin\left(\frac{\alpha}{2}\right)\right],$$

$$\sin\left(\frac{\alpha}{2}\right) = \frac{\Delta}{\sqrt{2\Xi^2 + 2\Delta^2 + 2\Xi\sqrt{\Xi^2 + \Delta^2}}}, \tag{9}$$

$$\cos\left(\frac{\alpha}{2}\right) = \frac{1}{2}\sqrt{2 + 2\frac{\Xi}{\sqrt{\Xi^2 + \Delta^2}}}.$$

The steady-state solution becomes unstable whenever K has an imaginary part since the perturbation then grows exponentially with the intensity given by the growth rate or the MI gain defined as $g(\Omega) \equiv 2\text{Im}(K)$ [6] as

$$g(\Omega) = C_{k,i} + \frac{\Delta(\Xi^2 + \Delta^2)^{1/4}}{\sqrt{2\Xi^2 + 2\Delta^2 + 2\Xi\sqrt{\Xi^2 + \Delta^2}}}. \tag{10}$$

We note that the MI gain does not depend on the fiber loss term α in (1) and the third-order dispersion term β_3. In fact, any odd-order β_j term does not contribute to the MI gain, however, it can influence the velocity and the propagation direction of the soliton induced by the MI [14]. It is interesting to find that the gain in (10) is proportional to Ω^4 due to the presence of the fourth-order dispersion term in (1). Thus, we expect a more complex gain spectrum in comparison with the higher-order nonlinear Schrödinger equation only containing the second and third dispersion terms. Under the condition that the nonlinear response of the medium is non-resonant and instantaneous so that we can ignore other phenomena appearing like self-steepening and the self-frequency shifting through the Raman effect, i.e, ignoring the second and third terms in (1), the author [14]

has previously derived the MI gain as

$$g(\Omega) = \frac{|\beta_4\Omega|}{12}\left\{-\left(\Omega^2 + 12\frac{\beta_2}{\beta_4}\right)\left[\Omega^4 + 12\frac{\beta_2}{\beta_4}\Omega^2\right.\right.$$

$$\left.\left. + 48\frac{P(\gamma_1 + 2\gamma_2 P)}{\beta_4}\right]\right\}^{1/2}, \tag{11}$$

from which four types of MI gain spectra as functions of γ_1, γ_2, β_j, and P have been classified. Those MI gain spectra are shown to exist both for the anomalous dispersion ($\beta_2 < 0$ with $\beta_4 > 0$) and for the normal dispersion ($\beta_2 > 0$ with $\beta_4 < 0$) showing four MI peaks which resemble to the cross-phase modulation term [14]. It is also shown that the power is related to the cubic and quintic nonlinear terms.

Now we turn to the characteristics of the MI gain spectrum under some specific physical conditions. In general, the nonlinear coefficients γ_i ($i = 1, 2$) are sensitive to the properties of optical fibers, which can be estimated from

$$\gamma_i = \frac{2\pi n_j}{\lambda A_{\text{eff}}}, \tag{12}$$

where n_j ($j = 2, 4$) are the nonlinear refractive index coefficients, λ is the typical wavelength for optical fiber ($\lambda \approx 1.55 \ \mu\text{m}$), and A_{eff} is the effective fiber core area (see [6] for detail) which varies from 20 μm^2 to 100 μm^2. As examples, in the following analysis we take the typical values for n_2 and n_4 as: $n_2 = 2 \times 10^{-17} \ \text{m}^2/\text{W}$ and $n_4 = -5 \times 10^{-31} \ \text{m}^4/\text{W}^2$ for an AlGaAs waveguide; $n_2 = (10^{-17} \sim 10^{-18}) \ \text{m}^2/\text{W}$ and $n_4 = -(10^{-28} - 10^{-29}) \ \text{m}^4/\text{W}^2$ for semiconductor doped and double-doped optical fibers [18]. Thus, we adopt $|\gamma_1| = (1 - 100) \ \text{W}^{-1}/\text{km}$ and $|\gamma_2| = (1 \times 10^{-4} - 5 \times 10^{-7}) \ \text{W}^{-2}/\text{km}$, where the absolute denotes the possibility of either positive or negative signs of γ_j depending on the properties of optical fibers. As an example, if the nonlinear coefficients γ_1 and γ_2 have the same sign, then the fifth-order nonlinearity only supports the self-focusing or defocusing effect of the medium. However, in the case $\gamma_1\gamma_2 < 0$, the role of the γ_2 nonlinearity can be essential for the physical features and the stability of the optical soliton propagation [19]. Finally, we assume the typical values for β_j as $\beta_2 \approx \pm(20 - 60) \ \text{ps}^2/\text{km}$, $\beta_3 \approx (0.1 - 1) \ \text{ps}^3/\text{km}$, and $\beta_4 \approx \pm(10^{-3} - 10^{-1}) \ \text{ps}^4/\text{km}$. In the following analysis, we omit the units of the coefficients.

Since it is difficult to analytically investigate the characteristics of the MI gain function (10), we calculate K in (9) numerically for various model coefficients. Figure 1 shows the MI gain as functions of
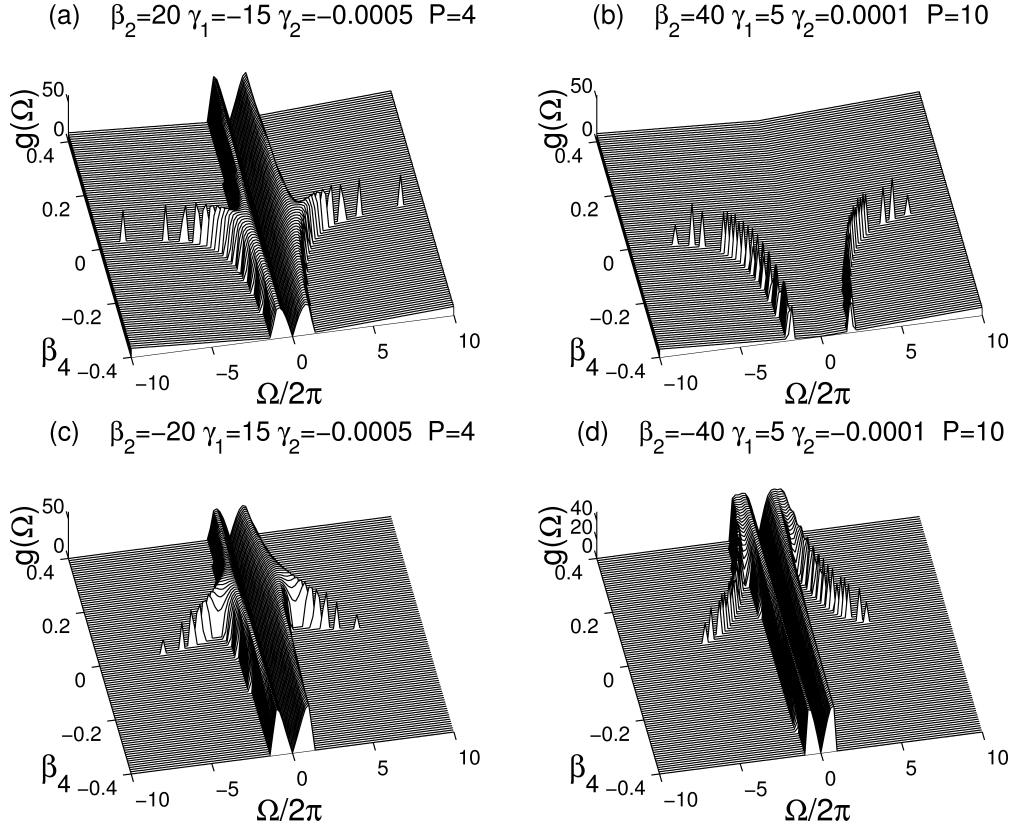
(a) $\beta_2=20$ $\gamma_1=-15$ $\gamma_2=-0.0005$ P=4

(b) $\beta_2=40$ $\gamma_1=5$ $\gamma_2=0.0001$ P=10

(c) $\beta_2=-20$ $\gamma_1=15$ $\gamma_2=-0.0005$ P=4

(d) $\beta_2=-40$ $\gamma_1=5$ $\gamma_2=-0.0001$ P=10

Fig. 1. Gain spectra as functions of β_4 and Ω for different power, dispersion, and nonlinear coefficients. (a) Four gain peaks exist for the normal dispersion regime when both $\beta_2\beta_4 < 0$ and $\gamma_1\gamma_2 > 0$ are satisfied. For $\beta_2\beta_4 > 0$, only two gain peaks remain. Note that the peak to peak separation increases for $\beta_4 \to 0$. A small fourth-order dispersion term results in two additional gain peaks. (b) Only two gain peaks appear if $\beta_2\beta_4 < 0$, $\gamma_2 > 0$ and $\gamma_4 > 0$ are satisfied. (c) Similarly four peaks are shown for the anomalous dispersion regime when $\beta_2\beta_4 < 0$ and $\gamma_1\gamma_2 < 0$ are satisfied. (d) Similar to (c) but having stronger dispersion coefficient and power.

β_4 and Ω with fixed β_2 and P. The gain is sensitive to the sign and strength of the dispersion and nonlinear coefficients. Figures 1a and 1b show the spectra for the cases of the normal dispersion regime $\beta_2 = 20$ and $\beta_2 = 40$, respectively. Four gain peaks are shown in Figure 1a as $\beta_4 \to 0$ when $\gamma_1 < 0$ and $\gamma_2 < 0$. Interestingly, the fact that the gain peaks move away from the center and the peaks at lower frequencies disappear resembles the XPM induced gain spectrum in the normal dispersion regime (see [6] for details), occuring when two beams with orthogonal polarizations propagate simultaneously [6, 8]. On the other hand, only two gain peaks appear for $\gamma_1 > 0$ and $\gamma_2 > 0$ as shown in Figure 1b. We note that the gain in Figs. 1a and 1b increases linearly as the modulation frequency increases, i.e, the gain plane has a slope, when $\gamma_1\gamma_2 > 0$ is satisfied. We also find that the gain peak disappears in

Fig.1b when $\beta_2\beta_4 > 0$, while non-zero gain exists regardless of the signs of β_2 and β_4 as shown in Figure 1a. Figures 1c and 1d plot the gain spectra for the anomalous dispersion regime for $\beta_2 = -20$ and $\beta_4 = -40$, respectively. Four similar gain peaks as in Fig. 1a show up if $\beta_2 \to 0$ in case $\gamma_1\gamma_2 < 0$ is satisfied. On the other hand, a flat-top gain peak appears in Fig. 1d as $\beta_4 \to 0.4$. Note that the gain slope disappears in comparison with Figs. 1a and 1b when $\gamma_1\gamma_2 < 0$ is satisfied.

Figure 2 displays the MI gain as functions of β_2 and Ω with fixed β_4 and P. Two gain peaks appear (Fig. 2a) if $\beta_2\beta_4 > 0$ is satisfied, which separate as $\beta_2 \to 0$ and disappear in the $\beta_2\beta_4 < 0$ regime regardless of the signs of γ_1 and γ_2. In Fig. 2b, we find the appearance of the two gain peaks of the dispersion regime satisfying $\beta_2\beta_4 < 0$ for $\gamma_1 < 0$ and $\gamma_2 < 0$, and
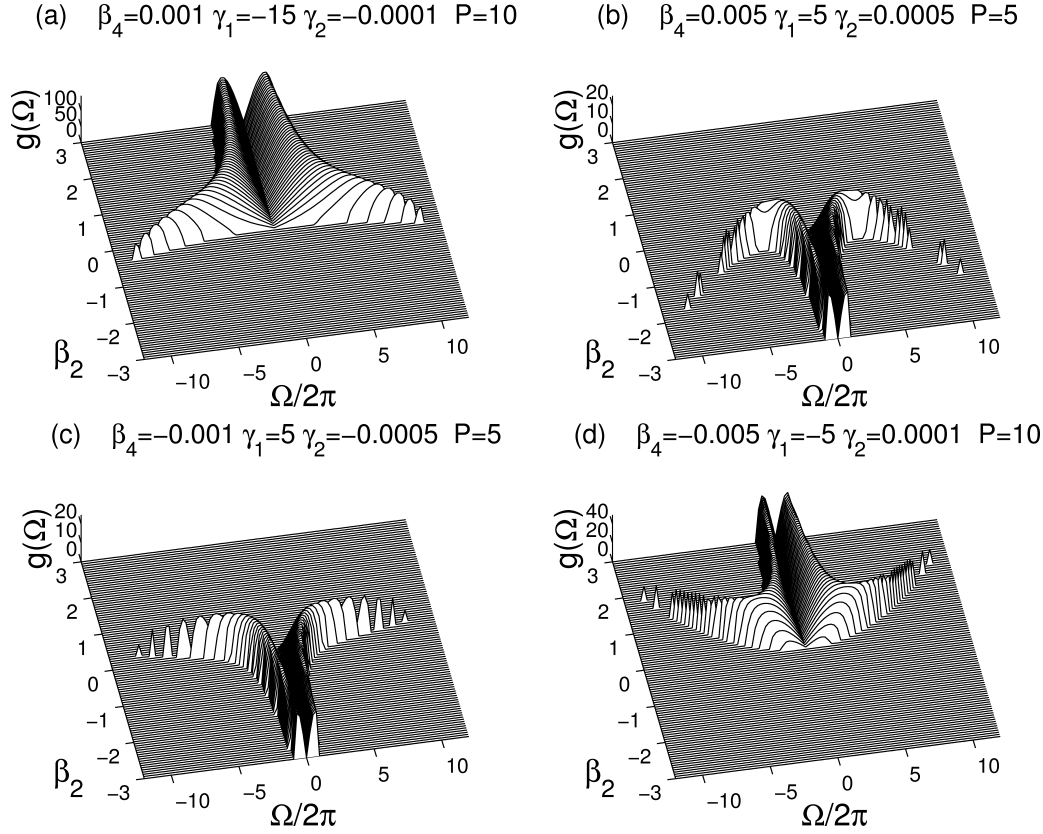
(a) β_4=0.001 γ_1=−15 γ_2=−0.0001 P=10

(b) β_4=0.005 γ_1=5 γ_2=0.0005 P=5

(c) β_4=−0.001 γ_1=5 γ_2=−0.0005 P=5

(d) β_4=−0.005 γ_1=−5 γ_2=0.0001 P=10

Fig. 2. Gain spectra as functions of β_2 and Ω for different power, dispersion, and nonlinear coefficients. (a) The gain peaks separate as $\beta_2 \to -0.5$ in the case of both negative nonlinear coefficients. (b) Four gain peaks appear for $-1.5 \leq \beta_2 \leq -0.5$ if both nonlinear coefficients are positive. Note that for $\beta_2\beta_4 > 0$ the gain vanishes. (c) Similar to (b) except $\gamma_1\gamma_2 < 0$ and $\beta_4 < 0$. Gain peak separation disappears as $\beta_2 \to -3$. (d) Similar to (c) except $\gamma_1\gamma_2 < 0$ and $\beta_4 < 0$. Gain peak separation disappears as $\beta_2 \to 0$.

four gain peaks at $-2 \leq \beta_2 < 0$. The gain spectrum in Fig. 2c is similar to Fig. 2b except that non-zero gain exists if $\beta_2\beta_4 > 0$ and $\gamma_1\gamma_2 < 0$. Finally, four gain peaks appear in Fig. 2d as $\beta_2 \to 2$ while $\beta_2\beta_4 < 0$ is satisfied.

3. Numerical Simulations of the Modulational Instability

In order to understand the dynamics of a CW beam propagation under the MI, (1) is solved utilizing the split-step Fourier method under periodic boundary condition [20]. Recently, Pitois and Milot [11] have experimentally investigated the influence of the fourth-order dispersion on the onset of scalar spontaneous MI in a single-mode fiber and demonstrated the evidence of a new MI spectral window due to a β_4 effect in the normal dispersion regime. The role of the fourth-order

dispersion for the MI in the case of normal dispersion has also been investigated in [12]. The purpose of the present work is to investigate the dynamics of the solitons induced by the MI in the regimes of the anomalous dispersion ($\beta_2 < 0$) with $\beta_4 > 0$ and the normal dispersion ($\beta_2 > 0$) with $\beta_4 < 0$.

We consider an incident field at the launch plane $z = 0$ into the nonlinear medium of the form

$$A(0, \tau) = \sqrt{P_0}[1 + \varepsilon_m \cos(\Omega_m \tau)], \qquad (13)$$

where ε_m is the normalized modulation amplitude and Ω_m is the angular frequency of a weak sinusoidal modulation imposed on the CW beam, which can be determined from the above gain spectrum when γ_j and β_j are fixed. In the following simulations, we set the fiber loss term $\alpha = 0$ since it does not contribute to the MI gain.
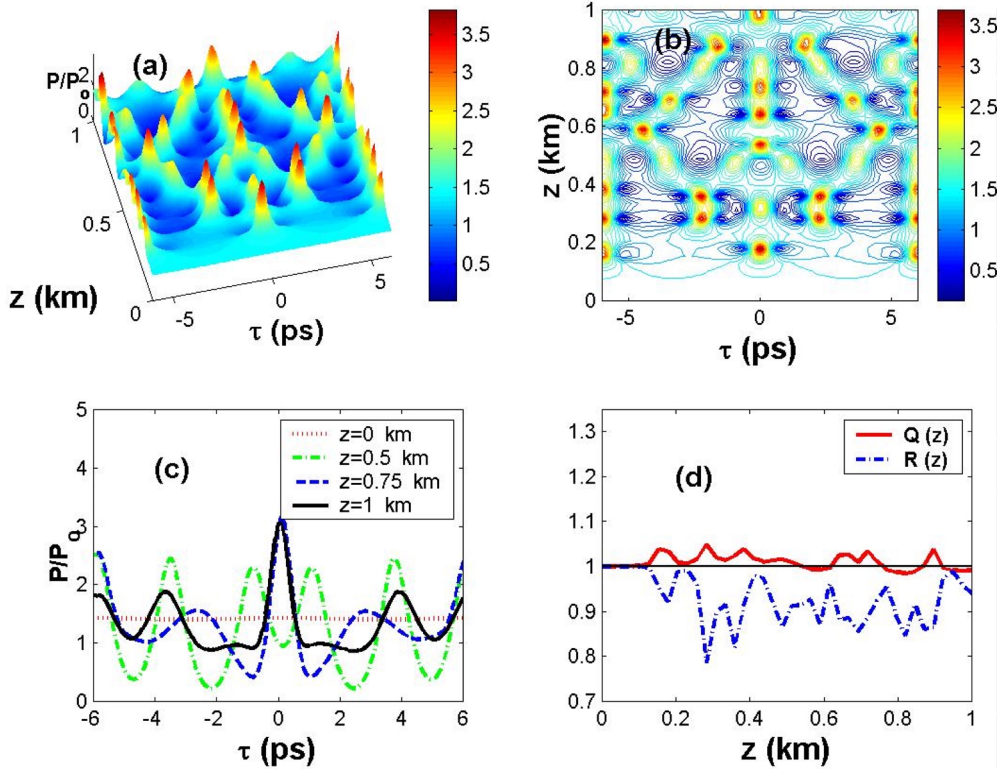
Fig. 3. Development of the MI in the anomalous dispersion regime. (a) Evolution of the relative power, i.e., $P(z,t)/P_0$, for the given perturbed initial profile $A(0,\tau) = \sqrt{P_0}[1+\varepsilon_\mathrm{m}\cos(\Omega_\mathrm{m}\tau)]$, where the modulation frequency $\Omega_\mathrm{m} = 1$ THz, $\varepsilon_\mathrm{m} = 0.01$, $\beta_2 = -20, \beta_3 = 0.04$, $\beta_4 = 0.005$, $\gamma_1 = -20$, $\gamma_2 = 4\times10^{-3}$, and $T_\mathrm{R} = 0.03$. Note the periodic occurrences of the solitons induced by the MI. (b) The contour plot shows a symmetry about $\tau = 0$ as the consequence of the periodic boundary condition. (c) Snapshots of the relative power due to the MI. The initial perturbed profile develops to the soliton with the sidebands at $z = 1$ km. (d) $Q(z)$ and $R(z)$ represent the changes of the energy and mass, respectively, along the evolution distance z. The peaks (solid curve) or dips (dot-dashed curve) are the distances where the solitons are induced by the MI.

3.1. Anomalous Dispersion ($\beta_2 < 0$) with $\beta_4 > 0$

The results of the numerical simulations of the MI in the anomalous dispersion regime are presented in Figs. 3 and 4. As an example, by choosing $\beta_2 = -20, \beta_3 = 0.04, \beta_4 = 0.005, \gamma_1 = -20, \gamma_2 = 4\times10^{-3}$, and $T_\mathrm{R} = 0.03$ fs, which belong to the coefficients of the MI spectrum in Fig. 1c, with $\Omega_\mathrm{m} = 1$ THz and $\varepsilon_\mathrm{m} = 0.01$, we plot in Fig. 3a the evolution of the relative peak power $P(z,\tau)/P_0$, where $P(z,\tau) \equiv |A(z,\tau)|^2$ and $P_0 \equiv |A(z,0)|^2$. The typical periodic occurrence of stable soliton-like pulses (hereafter we denote them as solitons) induced by the MI along the evolution distance is observed, even in the presence of the higher-order dispersion terms, in contrast to the numerical results of [13] where non-zero third- and fourth-order dispersion terms lead the initial waves to turbulent

states. The reason for the existence of the soliton in this case is a complicated interplay between the non-linear and higher-order dispersion terms. As shown in the contour plot of Fig. 3b, the soliton evolution shows a perfect symmetry about $\tau = 0$ as a consequence of the imposed periodic boundary condition. The snapshots of the relative peak in Fig. 3c show the initial perturbed CW developing into a soliton with sidebands at $z = 1$ km, which is similar to the result investigated in the context of the supercontinuum generation by the MI [12]. To better understand the dynamical behavior of the soliton along the evolution distance z, we calculate the total energy and mass (or the area under $|A(z,\tau)|$) defined as $\mathcal{E}(z) \equiv \int_{-\infty}^{\infty}|A(z,\tau)|^2\mathrm{d}\tau$ and $\mathcal{M}(z) \equiv \int_{-\infty}^{\infty}|A(z,\tau)|\mathrm{d}\tau$, respectively, and plot $Q(z) \equiv \mathcal{E}(z)/\mathcal{E}(0)$ and $R(z) \equiv \mathcal{M}(z)/\mathcal{M}(0)$ in Figure 3d. An interesting feature is that the peaks in $Q(z)$ (solid
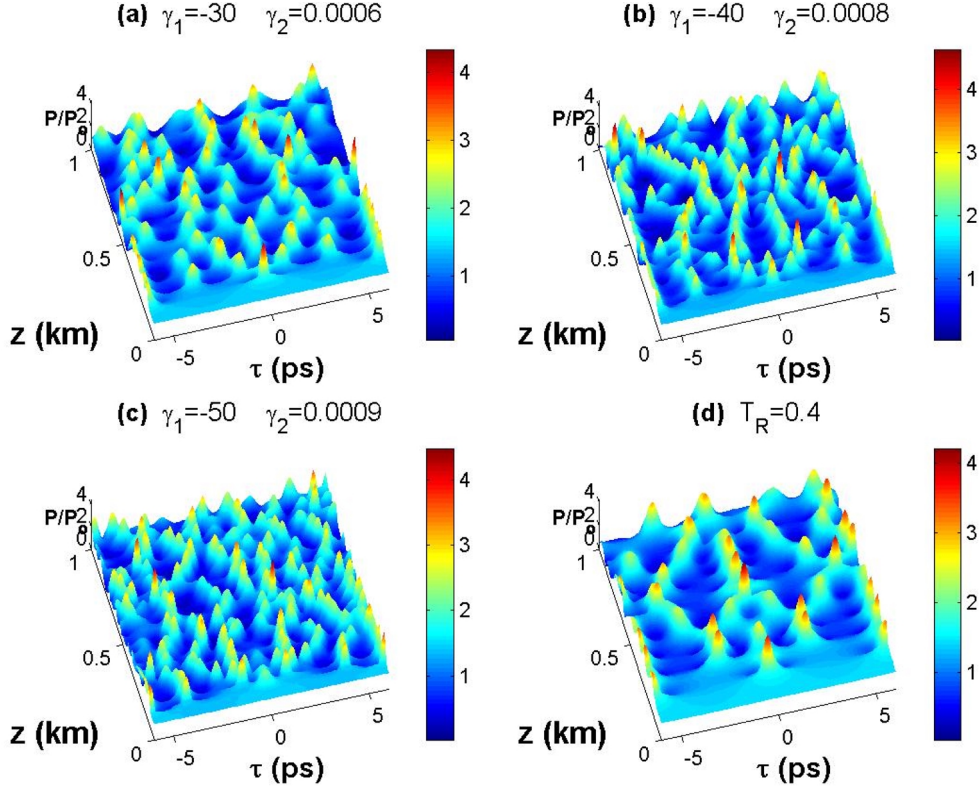
Fig. 4. Evolutions of the solitons induced by the MI for the same coefficients as in Fig. 3 but varying γ_1 and γ_2 or the intrapulse Raman scattering term T_R. (a) – (c) As both strength of γ_1 and γ_2 increase, more solitons interacting with each other along the evolution distance are shown. Note $\gamma_1 < 0$ and $\gamma_2 > 0$. (d) In comparison with Fig. 3a, the stronger intrapulse Raman scattering term does not alter the dynamics of the solitons.

curve) or the dips in $R(z)$ (dot-dashed curve) represent the regions at which the soliton is induced by the MI and they occur at the same evolution distance. In particular, we find $Q(z) \approx R(z) \approx 1.0$ at $z \simeq 0.22$ km and $z \simeq 1.0$ km, where the system returns to the initial perturbed state.

We now investigate the evolution of the MI with the same coefficients as in Fig. 3 but varying γ_1 and γ_2 or T_R. Figures 4a and 4c show the effects of the nonlinear terms on the behavior of the injected CW. As both strength of γ_1 and γ_2 increase, we observe the appearance of more MI-induced solitons which subsequently undergo mutual interaction with each other along the evolution distance, as shown in Figures 4a and 4c. As the strength of the nonlinear terms further increases, i.e, $|\gamma_1| \geq 120$ and $|\gamma_2| \geq 0.0001$, the initial CW eventually turns into a chaotic state, which has been numerically confirmed. However, in comparison with Fig. 3a, the stronger intrapulse Raman scattering term does not alter the dynamics of the solitons, which can be related

to the fact that the T_R term does not affect the supercontinuum generation [12].

3.2. Normal Dispersion ($\beta_2 > 0$) with $\beta_4 < 0$

The simulated evolutions of the MI in the normal dispersion regime are displayed in Figs. 5 and 6. As an example, we set $\beta_2 = 30$, $\beta_3 = 0.3$, $\beta_4 = -0.002$, $\gamma_1 = 20$, $\gamma_2 = 4 \times 10^{-3}$, and $T_R = 0.03$, which belong to the coefficients of the MI spectrum type in Fig. 1b, with $\Omega_m = 1$ THz and $\varepsilon_m = 0.01$. In contrast to the results in Figs. 3a and b, due to the stronger β_3 term, the soliton in Fig. 5a travels towards the right, which can be more clearly demonstrated in the asymmetric contour plot in Figure 5b. This shows that even though the β_3 term does not contribute to the MI gain, it can alter the propagation direction of the soliton in the presence of both the higher-order nonlinear and dispersion terms. The fact that the solitons attract each other and collide periodically along the evolution distance, which is
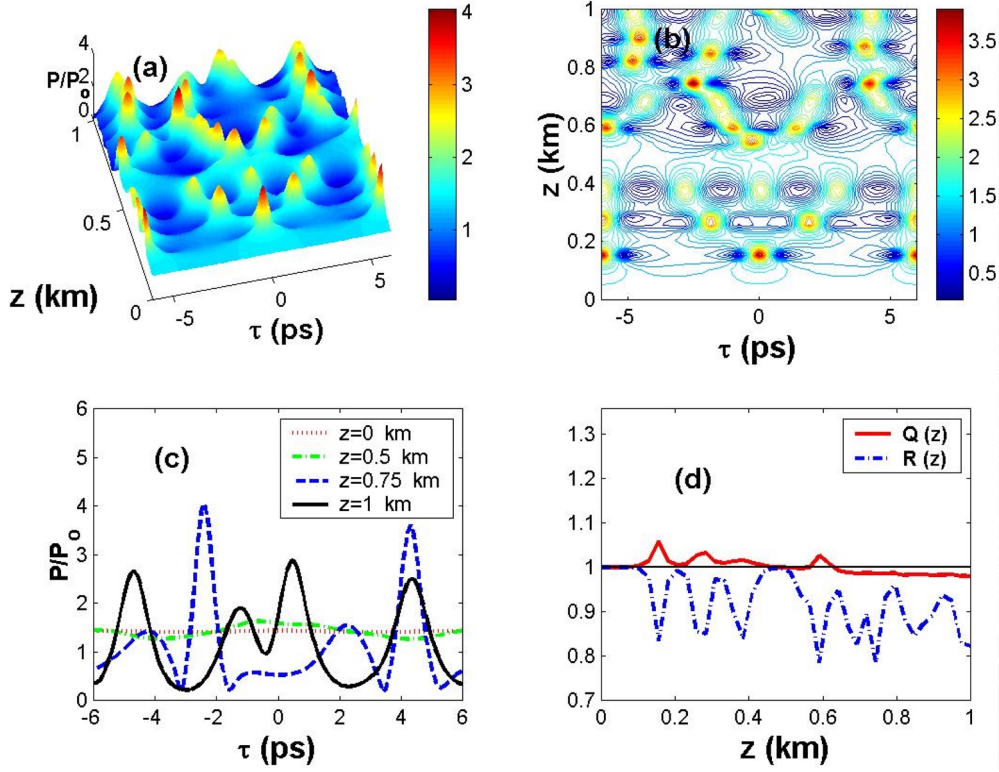
Fig. 5. Development of the MI in the normal dispersion regime. (a) Evolution of the relative power for $\beta_2 = 30$, $\beta_3 = 0.3$, $\beta_4 = -0.002$, $\gamma_1 = 20$, $\gamma_2 = 4 \times 10^{-3}$, and $T_R = 0.03$ with $\Omega_m = 1$ and $\varepsilon_m = 0.01$. Due to the strong β_3 term, the solitons in Fig. 5a travel towards the right in comparison with the result in Fig. 3a. The collision of the solitons along the evolution distance is shown. (b) The contour plot shows asymmetry about $\tau = 0$. (c) Snapshots of the solitons for various evolution distances. The snapshot at $z = 1$ km shows two interacting solitons (in the middle). (d) The peaks in $Q(z)$ (solid curve), which are anticorrelated with the dips in $R(z)$ (dot-dashed curve), represent the distance at which the soliton is induced by the MI.

similar to the collision of two solitons in-phase case in the context of the standard nonlinear Schrödinger equation [6], is demonstrated. As the consequence of a stronger β_3 term than that in Fig. 3, we find the snapshot of the two interacting solitons (in the middle) at $z = 1$ km as shown in Fig. 5c, instead of the formation of the sidebands. Figure 5d shows the peaks in $Q(z)$ (solid curve), which are anticorrelated with the dips in $R(z)$ (dot-dashed curve), representing the distances at which the solitons are produced by the MI. However, the energy of the system is more rapidly decreasing above $z \simeq 0.65$ km due to the stronger β_2 term in comparison with that of Figure 3d.

The simulations of the initial CW with the same coefficients as in Fig. 3 but with varying γ_1 and γ_2 are presented in Figure 6. As both $\gamma_1 > 0$ and $\gamma_2 > 0$ increase, we observe some highly peaked solitons which undergo more active mutual interaction as found in

Figs. 4a and b, due to the presence of the strong nonlinear terms. On the other hand, for the case of further increased γ_1 but γ_2 values as in Fig. 4c under the constraint that $\gamma_1 > 0$ and $\gamma_2 < 0$, the dynamical complexity of the solitons increases by showing a chaotic behavior. However, for both negative nonlinear coefficients in Fig. 4d, the initial CW decays to a constant background.

4. Conclusions

In this paper we have derived an analytic expression of the MI gain for the generalized nonlinear Schrödinger equation with a third- and fourth-order dispersion and cubic-quintic nonlinear terms in (1), describing the propagation of intense femtosecond optical pulses in a medium which exhibits a parabolic nonlinearity law [6, 9, 10 – 12]. We have shown in Figs. 1 and 2 that the MI gain can exist even in the normal
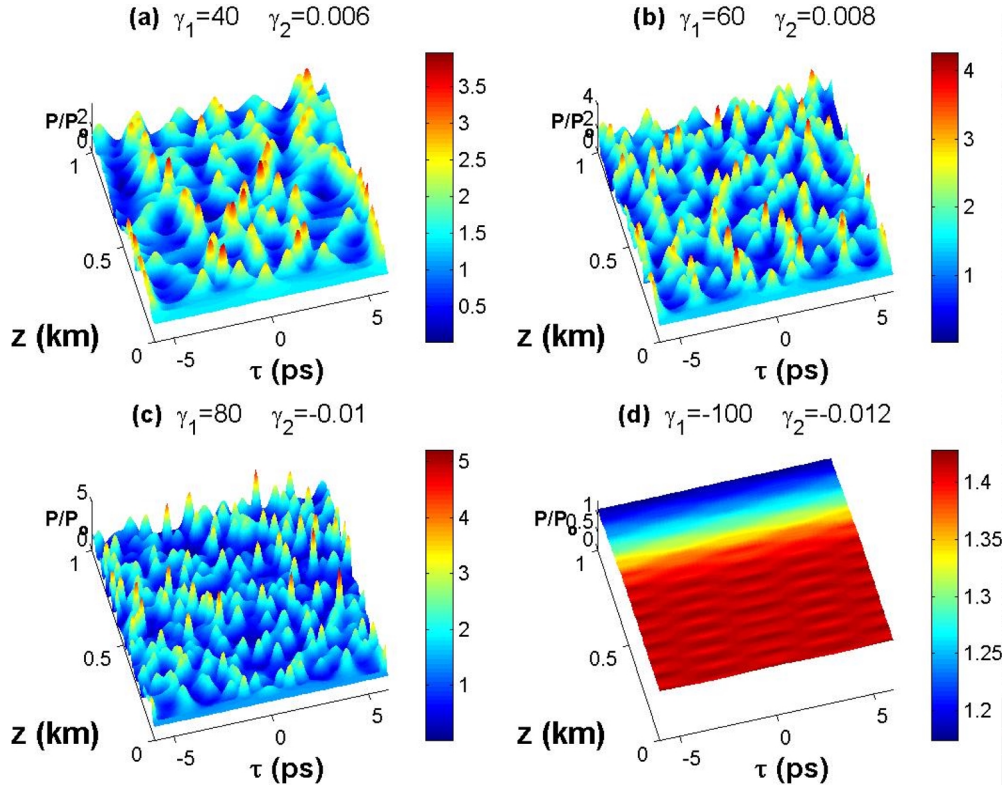
Fig. 6. Evolutions of the solitons induced by the MI for the same coefficients as in Fig. 3 but varying γ_1 and γ_2. (a), (b) As both $\gamma_1 > 0$ and $\gamma_2 > 0$ increase, higher peaked solitons with active mutual interactions appear. (c) For further increased values with $\gamma_1 > 0$ and $\gamma_2 < 0$ constraint, the dynamical complexity of the solitons increases by showing a chaotic behavior. (d) For both negative nonlinear coefficients in Fig. 4d, the initial CW is shown to decay to a constant background.

dispersion medium, depending on the strength of the higher-order dispersion and nonlinear terms, in contrast to the NLS equation in which the MI gain occurs only in the anomalous dispersion regime. In particular, the gain spectra in Fig. 2c in the anomalous dispersion regime for the nonlinear coefficients ($\gamma_1 > 0$ and $\gamma_2 < 0$) may be experimentally testable since the nonlinear medium has been recently realized in organic materials such as polydiacetylene paratoluene sulfonate (PTS) [21].

Numerical simulations have been performed to investigate the effects of the higher-order nonlinear and dispersion terms on the evolution of the steady-state initial CW under the modulationally perturbed field. In Figs. 3 and 4, we have simulated the evolutions of the MI in the anomalous dispersion regime ($\beta_2 < 0$) with $\beta_4 > 0$. The typical periodic occurrences of the solitons induced by the MI along the evolution distance were found in Fig. 3 even in the presence of the higher-order dispersion terms, in contrast to the numerical re-

sults of [13] in which the non-zero third- and fourth-order dispersion terms lead the initial waves to turbulent states, due to a complicated interplay between the nonlinear and the higher-order dispersion terms. An interesting feature in Fig. 3d is that the peaks in $Q(z)$ (solid curve) or the dips in $R(z)$ (dot-dashed curve) represent the distances at which the solitons are produced by the MI. It was found that as the strength of the nonlinear terms increases, more MI-induced solitons appear which undergo mutual interactions with each other along the evolution distance as demonstrated in Figs. 4a – c, while the intrapulse Raman scattering term does not alter the dynamics of the soliton as shown in Figure 4d.

In Figs. 5 and 6, we have shown the evolutions of the MI in the normal dispersion regime ($\beta_2 > 0$) with $\beta_4 < 0$. For a strong β_3 term, the solitons in Fig. 5a were shown to travel towards the right, even though it does not contribute to the MI gain. We have found that as both $\gamma_1 > 0$ and $\gamma_2 > 0$ increase highly peaked solitons

with more active mutual interaction appear as shown in Figs. 4a and 4b, due to the presence of the strong nonlinear terms. However, for both negative nonlinear coefficients in Fig. 4d, the initial CW was shown to decay to a constant background.

[1] G. B. Whitham, Proc. R. Soc. **283**, 238 (1965).
[2] T. B. Benjamin and J. E. Feir, J. Fluid Mech. **27**, 417 (1967).
[3] V. I. Bespalov and V. I. Talanov, JETP Lett. **3**, 307 (1966).
[4] V. I. Karpman, JETP Lett. **6**, 277 (1967).
[5] T. Taniuti and H. Washimi, Phys. Rev. Lett. **21**, 209 (1968).
[6] G. P. Agrawal, Nonlinear Fiber Optics, Optics and Photonics, Academic Press, London 2001, and references therein.
[7] K. Tai, A. Hasegawa, and A. Tomita, Phys. Rev. Lett. **56**, 135 (1986).
[8] G. P. Agrawal, Phys. Rev. Lett. **59**, 880 (1987).
[9] S. L. Palacios and J. M. Fernández-Díaz, Opt. Commun. **178**, 457 (2000).
[10] S. L. Palacios and J. M. Fernández-Díaz, J. Modern Opt. **48**, 1691 (2001).
[11] S. Pitois and G. Millot, Opt. Commun. **226**, 415 (2003).
[12] A. Demircan and U. Bandelow, Opt. Commun. **244**, 181 (2005).

[13] A. G. Shagalov, Phys. Lett. A **239**, 41 (1998).
[14] W. P. Hong, Opt. Commun. **213**, 173 (2002).
[15] J. D. Harvey, R. Leonhardt, S. Coen, G. K. L. Wong, J. C. Knight, W. J. Wadsworth, and P. St. J. Russel, Opt. Lett. **28**, 2225 (2003).
[16] P. K. Shukla and J. J. Rasmussen, Opt. Lett. **11**, 171 (1986).
[17] M. J. Potasek, Opt. Lett. **12**, 921 (1987).
[18] G. I. Stegeman, A. Villeneuve, J. S. Aitchison, and C. N. Ironside, Nonlinear Integrated Optics and All-Optical Switching in Semiconductors, in: Fabrication, Properties and Applications of Low-Dimensional Semiconductors, NATO ASI Series, 3. High Technology, Vol. 3 (Eds. M. Balkanski, I. Yantchev), Oxford University Press, Oxford 1995, p. 145.
[19] S. Tanev and D. I. Pushkarov, Opt. Commun. **141**, 322 (1997).
[20] J. A. C. Heideman and B. M. Herbst, SIAM J. Numer. Anal. **23**, 485 (1986).
[21] B. L. Lawrence and G. I. Stegeman, Opt. Lett. **23**, 591 (1998).